ACS APPLIED MATERIALS & INTERFACES

Research Article

www.acsami.org

Si Nanowires Organic Semiconductor Hybrid Heterojunction Solar Cells Toward 10% Efficiency

Lining He,[†,‡,§] Changyun Jiang,[‡] Hao Wang,[†] Donny Lai,[†,§] and Rusli*[,†,§]

[†]Nanofabrication Center, School of Electrical and Electronic Engineering, Nanyang Technological University, 50 Nanyang Avenue, Singapore 639798

[‡]Institute of Materials Research and Engineering, A*STAR, 3 Research Link, Singapore 117602

[§]CINTRA CNRS/NTU/THALES, UMI 3288, Research Techno Plaza, 50 Nanyang Drive, Border X Block, Level 6, Singapore 637553

ABSTRACT: High-efficiency hybrid solar cells are fabricated using a simple approach of spin coating a transparent hole transporting organic small molecule, 2,2′,7,7′-Tetrakis-(N,N-di-4-methoxyphenylamino)-9,9′-spirobifluorene (Spiro-OMeTAD) on silicon nanowires (SiNWs) arrays prepared by electroless chemical etching. The characteristics of the hybrid cells are investigated as a function of SiNWs length from 0.15 to 5 μm. A maximum average power conversion efficiency of 9.92% has been achieved from 0.35 μm length SiNWs cells, despite a 12% shadowing loss and the absence of antireflective coating and back surface field enhancement. It is found that enhanced aggregations in longer SiNWs limit the cell performance due to increased series resistance and higher carrier recombination in the shorter wavelength region. The effects of the Si substrate doping concentrations on the performance of the cells are also investigated. Cells with higher substrate doping concentration exhibit a significant drop in the incident photons-to-current conversion efficiency (IPCE) in the near infrared region. Nevertheless, a promising short circuit current density of 19 mA/cm^2 and IPCE peak of 57% have been achieved for a 0.9 μm length SiNWs cell fabricated on a highly doped substrate with a minority-carrier diffusion length of only 15 μm. The results suggest that such hybrid cells can potentially be realized using Si thin films instead of bulk substrates. This is promising towards realizing low-cost and high-efficiency SiNWs/organic hybrid solar cells.

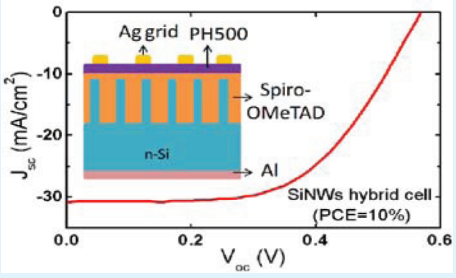

KEYWORDS: *silicon nanowires, organic semiconductor, hybrid solar cell, hybrid heterojunction, small molecule, conductive polymer*

1. INTRODUCTION

With soaring cost and increasing demand for energy, compounded with the problem of global warming due to greenhouse gases, it has become imperative to develop renewable clean energy resources such as solar energy. For solar energy to become a viable energy alternative, solar cells need to have high efficiency and yet be cost effective. Recently, there has been growing interest in the development of solar cells incorporated with silicon nanostructures, especially silicon nanowires (SiNWs),[1−9] because of their unique electrical and optical characteristics that can potentially result in higher cell efficiency and lower cost. Vertically aligned SiNWs solar cells have been shown to be less sensitivity to impurities[10] and posses superior charge separation capability which allows the use of low quality Si with shorter minority-carrier diffusion length. The outstanding light absorption property[5,11−13] of SiNWs has also been shown to significantly reduce the thickness of Si needed. In addition, as compared to other photovoltaic materials such as CdS, CdSe,[14,15] and ZnO[16] nanowires, SiNWs have wider absorption spectrum (400−1200 nm) and higher conductivity and are environmental friendly. Increasingly, more attention has been devoted to SiNWs/organic semiconductor hybrid cells instead of SiNWs all inorganic cells. Such hybrid cells can potentially offer the combined advantages of SiNWs such as high carrier mobility, and organic semiconductors such as low temperature solution processability and mechanical flexibility, and lead to a new generation of high-efficiency and low-cost solar cells.

Previously, SiNWs were embedded into light-absorbing polymer poly(3-octylthiophene) (P3OT),[17] forming solar cells with unsatisfactory power conversion efficiency (PCE) of less than 1%. Recently, hybrid cells were reported with a maximum PCE of up to 9% using SiNWs and a transparent polymer, poly(3,4-ethylenedioxy-thiophene): poly-(styrenesulfonate) (PEDOT).[7,18−20] As the polymer chains of PEDOT are too large to infiltrate into the small gaps inside the SiNWs arrays, incomplete coverage of the SiNWs surfaces by the PEDOT is expected. More recently, a hybrid structure based on heterojunction formed between SiNWs and a light-absorbing polymer, poly(3-hexylthiophene) (P3HT), was reported to achieve a maximum PCE of 5.9%.[8] Nevertheless, the performance is not optimized because many excitons generated in the P3HT will recombine before reaching the heterojunction due to their short minority-carrier diffusion

Received: December 24, 2011
Accepted: March 6, 2012
Published: March 6, 2012

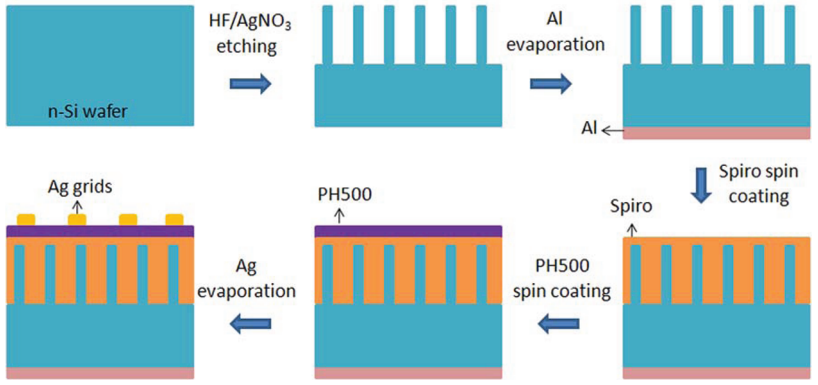

Figure 1. Schematic diagrams of the fabrication process of SiNWs/Spiro-OMeTAD hybrid solar cell.

length of only 3−10 nm.[21−23] This was indeed shown in the incident photon-to-current conversion efficiency (IPCE) spectrum where there was a significant drop in the IPCE at the maximum absorption of the P3HT film of 560 nm.[8] Besides, P3HT also suffers from the same problem of having long polymer chains, as in the case of PEDOT. Recently, we have reported a new SiNWs/organic hybrid structure[9] by introducing a transparent hole conducting small molecule, 2,2′,7,7′-Tetrakis-(N,N-di-4-methoxyphenylamino)-9,9′-spirobifluorene (Spiro-OMeTAD), whose small molecular size[24−26] enables it to infiltrate well into the small gaps among the SiNWs arrays and hence maximize the area of the heterojunction. We reported planar Si and 0.35 μm SiNWs hybrid cells with PCE of 5.6% and 10.3%, respectively, and to the best of our knowledge, the latter is the highest that has ever been reported for SiNWs/organic hybrid cells.[9] In this work, SiNWs/Spiro-OMeTAD hybrid cells fabricated with different SiNWs lengths ranging from 0.15 μm to 5 μm have been investigated. It is found that the cells with SiNW length of 0.35 μm show the highest average PCE and short circuit current density (J_{sc}) of 9.92% and 30.7 mA/cm^2, respectively. In contrast, those cells with longer SiNWs suffer a sharp drop in both the PCE and J_{sc}, due to their higher carriers recombination and series resistance. We have also studied SiNWs hybrid cells fabricated on Si substrates with different doping concentrations of 1×10^{15} cm^{-3}, 4×10^{18} cm^{-3} and 4×10^{19} cm^{-3}. A promising J_{sc} of 19 mA/cm^2 is obtained for a hybrid cell with doping concentration of 4×10^{18} cm^{-3}, which corresponds to minority-carrier diffusion length of 15 μm. This demonstrates that such SiNWs hybrid cells can also be potentially fabricated using thin film Si instead of bulk Si substrates.

2. EXPERIMENTAL SECTION

Fabrication of SiNWs/Organic Hybrid Solar Cells. The entire fabrication process is shown in Figure 1. Vertically aligned, single-crystal SiNWs arrays were fabricated on 2−4 Ω cm N-type Si wafers by electroless chemical etching method in a solution of hydrofluoric (HF) acid and silver nitrate ($AgNO_3$).[2] The concentration of HF and $AgNO_3$ were 4.6 M and 0.02 M, respectively. The etch time was varied to fabricate SiNWs with lengths (L) of 0.15, 0.35, 0.9, 1.2, 1.5, 2.7, 3.5, and 5 μm. After etching, the as-prepared SiNWs were soaked in concentrated nitric acid for at least 30 min to dissolve the tree-like silver dendrites. Then all the samples were immersed in 5% aqueous HF to remove any oxide. After that, a 250 nm thick aluminum was deposited by electron-beam evaporation onto the backside of the Si substrates to form the rear contact. Spiro-OMeTAD (Merck, Germany) dissolved in chlorobenzene was then spin coated onto the SiNWs arrays at 2000 rpm to form SiNWs/Spiro-OMeTAD core−sheath heterojunction structure. Following that, the films were dried for 24 h at room temperature in a drybox. Highly conductive PEDOT:PSS (Clevios PH500) mixed with 5 wt % dimethyl sulfoxide (DMSO) was spin-coated on top of the Spiro-OMeTAD covered SiNWs and then annealed at 110 °C for 10 min at atmosphere to dry the PH500 film. Finally, silver metal grid was deposited on top of the PH500 layer by electron-beam evaporation through a shadow mask to complete the cells each with an area of 0.95 cm^2. The fraction of the silver grid shading area is 12%. The fabrication process of the hybrid cells with 0.9 μm SiNWs on Si substrates with three doping concentrations of 1×10^{15} cm^{-3}, 4×10^{18} cm^{-3}, and 4×10^{19} cm^{-3} is exactly the same as just described.

Characterization. The nanoscale surface and cross-sectional topography of the SiNWs were measured using field-emission scanning electron microscopy (FESEM) (LEO 1550 Gemini). The reflectance spectra of the SiNWs arrays coated with organic materials were characterized using an integrating sphere by a PerkinElmer Lambda 950 UV/Vis/NIR spectrophotometer system. The photovoltaic current density-voltage ($J-V$) characteristics of the cells were measured with a Keithley 2400 Source-Meter unit under 100 mW/cm^2 illumination (AM 1.5G) from a solar simulator (San-EI electric). The intensity of the light source was determined by a calibrated Si reference cell which is traceable both to the National Renewable Energy Laboratory (NREL), and to the International System of Units (SI). The incident photon-to-current conversion efficiency (IPCE) was measured with a characterization system consisting of a Xenon lamp, a chopper controller, a monochromator, and a lock-in amplifier.

3. RESULTS AND DISCUSSION

Characterization of SiNWs/Organic Hybrid Structure. Figure 2a−d shows the top-view SEM images of the SiNWs arrays with different L of 0.35, 1.5, 2.7, and 5 μm coated with

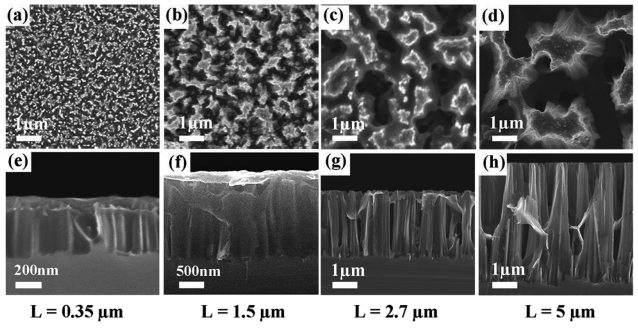

Figure 2. (a−d) Top view SEM images of the SiNWs coated with Spiro-OMeTAD with wire length (L) of 0.35, 1.5, 2.7, and 5 μm. (e−h) Corresponding cross-sectional view SEM images of these samples after they have been coated with the PH500 layer.

dx.doi.org/10.1021/am201838y | ACS Appl. Mater. Interfaces 2012, 4, 1704−1708

Spiro-OMeTAD. Figure 2e–h shows the corresponding cross-sectional view SEM images of these samples after they have been coated with the PH500 layer. From images e and f in Figure 2, it is clearly seen that Spiro-OMeTAD penetrates deep into the gaps among the SiNWs and encapsulates well the sidewalls of the SiNWs. Spiro-OMeTAD has been extensively used in solid-state dye sensitized solar cells where it has been demonstrated to exhibit an excellent pore-filling property in nanoporous TiO_2 film with pore size of around 30–50 nm, attributed to its small molecular size.[24−26] Figure 2a–d reveals that there are enhanced aggregations at the top of the SiNWs forming large SiNWs bundles as L increases. The aggregations reduce the gaps between the SiNWs inside each bundle, which may consequently lead to poor infiltration of Spiro-OMeTAD into the top portion of the bundled SiNWs. Meanwhile, the enhanced aggregations also result in larger void space of around 2–3 μm between the adjacent SiNW bundles as L is increased to 5 μm as shown in Figure 2h. As a result, these void spaces are not well filled up, despite that a very high Spiro-OMeTAD concentration of 180 mg/mL has been used. This leads to a very non-uniform surface contour of the PH500 layer coated on top.

Because the top surfaces of the cells with Spiro-OMeTAD coated on SiNWs are relatively rough, especially for longer L as shown in g and h in Figure 2, fabrication of a highly conductive and transparent electrode as the top anode to serve as the light window is a challenge. In this study, a highly transparent and conductive polymer PH500 was used together with a silver grid as the top anode. It was found to be very simple and effective. The PH500 mixed with 5 wt % DMSO has a good optical transmittance in the broad wavelength region of 350–1100 nm and a high conductivity of ~300 S/cm. It should be highlighted that the PH500/silver grid transparent electrode can also be fabricated by very simple, low-cost, and easily scalable methods such as slot coating or screen printing.

Effects of Wire Length on Cell Performance. The current density-voltage (J–V) characteristics of the hybrid cells with different L were measured under 100 mW/cm^2 illumination (AM 1.5G). Four cells were investigated for each value of L and the statistical distributions of the short circuit current density (J_{sc}), open circuit voltage (V_{oc}), fill factor (FF) and PCE are shown in Figure 3. In the following discussion, the cell parameters referred to are their average values. It is seen that the PCE increases with L and reaches a maximum of 9.92% at L = 0.35 μm (Figure 3b), beyond which it decreases continuously to 5.23% as L is further increased to 5 μm. The FF increases from 52% to 66.2% as L is increased from 0.15 to 2.7 μm. This could be attributed to enhanced carriers separation due to the increased junction area.[27,28] Besides, the nanoscale geometry of the SiNWs arrays has shortened the diffusion distance of photo-excited minority-carriers to the junction for charge separation.[29] However, beyond 2.7 μm, the FF drops continuously to 54%, which could be caused by the larger series resistance associated with the non-uniform surface morphology of the cells at larger L, as explained earlier.

As seen from Figure 3a, the J_{sc} and V_{oc} exhibit their maximum values of 30.72 mA/cm^2 and 0.57 V at L = 0.35 μm, respectively. As L is increased beyond 0.35 μm, J_{sc} and V_{oc} decrease monotonically to 18.85 mA/cm^2 and 0.48 V, respectively. Figure 4 shows the incident photon-to-current conversion efficiency (IPCE) spectra of SiNWs hybrid cells with different L. The IPCE increases with L up to a maximum value of 72.4% at 600 nm for L = 0.35 μm, but decreases

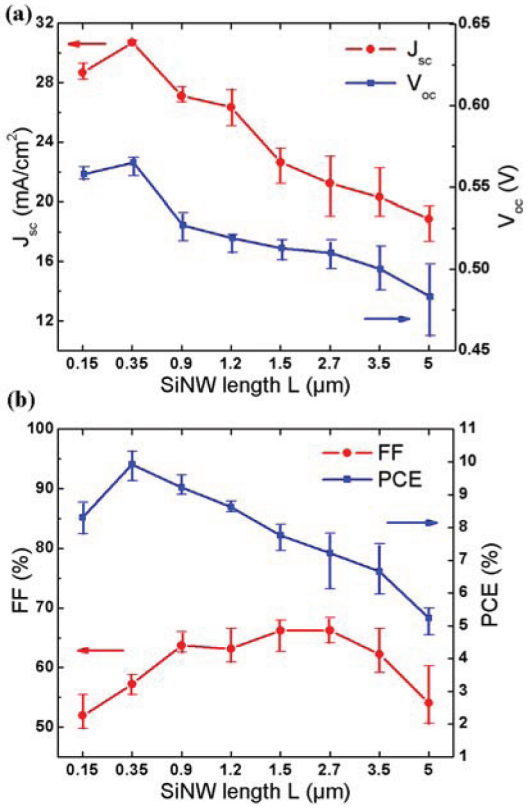

Figure 3. Average photovoltaic performances of (a) J_{sc} and V_{oc}, and (b) FF and PCE of the SiNWs/Spiro-OMeTAD solar cells as a function of SiNWs length (L).

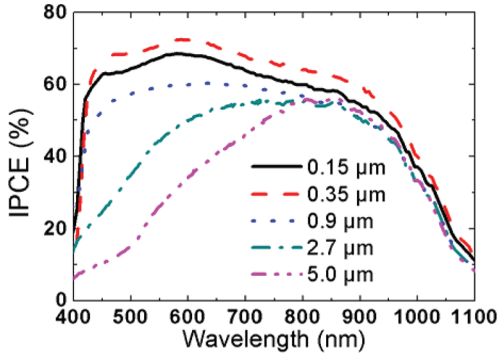

Figure 4. IPCE spectra of the SiNWs cells with different L of 0.15, 0.35, 0.9, 2.7, and 5.0 μm.

continuously as L is further increased, especially in the shorter wavelength region of 400–800 nm. This trend in the change of the IPCE is consistent with the variation of J_{sc} of the cells seen in Figure 3a.

To understand the change in J_{sc}, the reflectance of the SiNWs arrays with different L coated with Spiro-OMeTAD and PH500 were measured using an integrating sphere and shown in Figure 5. It is seen that the reflectance of the cells with L = 0.15 and 0.35 μm are generally lower compared to the cells with L = 0.9 μm, especially in the shorter wavelength region. We postulate that this might be due to the fact that Spiro-OMeTAD/PEDOT layer acts as an antireflective coating and already substantially reduces the reflectance of light. This antireflective effect may be stronger than the light trapping effect arising from SiNWs, and result in the reflectance not strongly

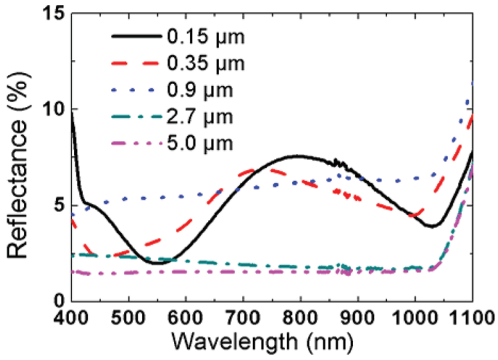

Figure 5. Reflection of SiNWs arrays coated with Spiro-OMeTAD and PH500 with different L of 0.15, 0.35 , 0.9 , 2.7, and 5.0 μm.

correlated to the SiNW length for shorter L. In addition, such cells with shorter L have better carrier collection efficiency because of the shorter hole travelling distance in the Spiro-OMeTAD along the axial direction of the SiNWs. The above two advantages lead to the higher IPCE observed and account for the higher J_{sc} seen for the cells with L = 0.15 and 0.35 μm. For the cells with L = 2.7 and 5.0 μm, it is noted that their reflectance drops substantially due to the more effective trapping of light by the longer SiNWs. Despite this, the IPCE of these cells are lower, which is indicative of a higher carrier recombination rate. A recent study has shown that there are indeed more surface defects for longer SiNWs prepared by metal-catalyst electroless etching, resulting in a shorter carrier lifetime and thus a higher carrier recombination rate.[30] Moreover, the enhanced aggregation for the longer SiNWs as shown in images c and d in Figure 2 would lead to poor infiltration and coverage of Spiro-OMeTAD on the SiNWs that are bundled together. As a result, for the shorter wavelength photons that are absorbed near the tips of the SiNWs, there is a very high recombination rate as there is no junction formed at the poorly coated SiNWs tips for carrier separation. This is indeed consistent with the IPCE results, where a tremendous drop in the shorter wavelength region is observed for the samples with longer L. In contrast, their IPCE spectra do not change as much near the infrared (NIR) region as most of the longer wavelength photons will be absorbed in the Si substrates because of their larger absorption depth. The minority-carrier holes generated will diffuse up to the bottom of the SiNWs and can be readily extracted at the SiNWs/Spiro heterojunction formed there because the bottom portion of the SiNWs has no aggregation and is well-coated by Spiro. The higher recombination rate in the cells with longer SiNWs is also consistent with the decrease in their V_{oc}, as seen in Figure 3a for L beyond 0.35 μm.

Effects of Si Substrate Doping Concentrations on Cell Performance. From our cell structure, it is expected that the bulk Si substrates will also contribute to optical absorption and hence photocurrent generated. To study the contribution of the Si substrates to the cell performance, Si wafers with three different doping concentrations of 1×10^{15} cm^{-3}, 4×10^{18} cm^{-3} and 4×10^{19} cm^{-3} were used to fabricate SiNWs/Spiro-OMeTAD hybrid cells with 0.9 μm wire length. As the doping concentration of the Si substrate determines the minority-carrier diffusion length,[31] these wafers allow us to mimic Si thin films with effective absorber thickness of 400 μm, 15 μm and 0.5 μm respectively. This study can also serve as a proof-of concept to demonstrate the feasibility of the SiNWs/Spiro-OMeTAD hybrid cells fabricated using Si thin film photovoltaic technology.

Figure 6 shows the $J-V$ characteristics of the hybrid cells with different different substrate doping concentrations under dark condition and simulated AM 1.5G irradiation at 100 mW/cm^2. Their photovoltaic parameters of J_{sc}, V_{oc}, FF, and PCE are summarized in Table I. It is seen that as the doping concentration is increased from 1×10^{15} to 4×10^{19} cm^{-3}, the PCE of the cell decreases significantly from 9.2% to 0.18%, as a result of drop in J_{sc}, V_{oc}, and FF. Figure 6a shows that there is an increase in the dark saturation current (J_0) for the heavier doped cells. The significant reduction in J_{sc} and increase in J_0 of the heavier doped cells accounts for the drop in their V_{oc} and FF. Figure 7 shows the IPCE spectra of the SiNWs hybrid cells with different substrate doping concentrations. It is seen that the IPCE peak decreases from 59.6% to 27% as the doping concentration increases from 1×10^{15} to 4×10^{19} cm^{-3}. The reduction in the IPCE is more drastic at the NIR region, attributed to the shorter minority-carrier diffusion length in the highly doped Si substrates. Most of the longer wavelength photons absorbed in the highly doped substrates will generate carriers that recombine before reaching the junction interface. It is worth noting that as compared to the cell with doping concentration of 1×10^{15} cm^{-3}, there is only a slight drop in

Table I. Summary of the Photovoltaic Parameters

doping concentration (cm^{-3})	J_{sc} (mA/cm^2)	V_{oc} (V)	FF (%)	PCE (%)
1×10^{15}	26.7	0.53	64.3	9.2
4×10^{18}	19	0.34	48.9	3.2
4×10^{19}	5.0	0.12	28.8	0.18

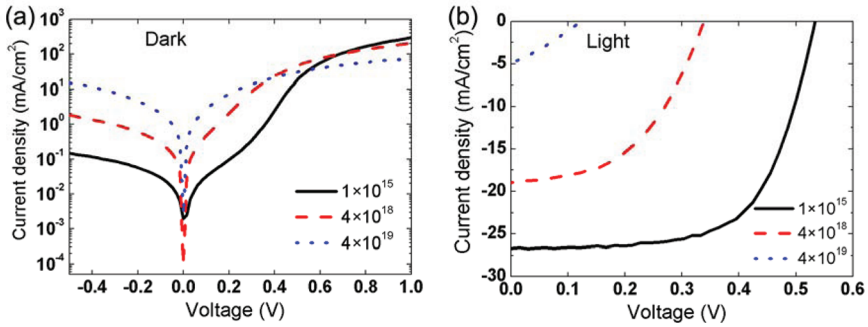

Figure 6. The current density-voltage ($J-V$) characteristics of the 0.9 μm SiNWs hybrid cells with different Si substrate doing concentrations of 1×10^{15} cm^{-3}, 4×10^{18} cm^{-3}, and 4×10^{19} cm^{-3} under (a) dark condition and simulated AM 1.5G irradiation at 100 mW/cm^2.

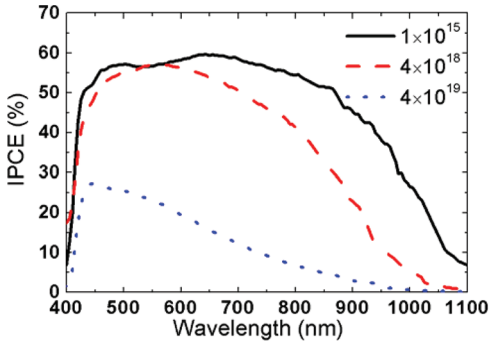

Figure 7. IPCE spectra of SiNWs hybrid cells with different Si substrate doing concentrations.

the IPCE at the shorter wavelength region for the cell with doping concentration of 4×10^{18} cm^{-3}, which corresponds to an effective Si absorber of 15 μm. Such cell achieves a promising IPCE peak of 57% and a J_{sc} of 19 mA/cm^2. However, its PCE is only 3.2%, which is ascribed to its poor V_{oc} and FF associated with its extremely high substrate doping concentration. Garnett et al.[5] has reported a similar result from SiNWs all inorganic solar cells, with SiNWs fabricated on a thin epitaxial Si layer deposited on a highly doped Si substrate. They achieved a V_{oc} greater than 0.5 V attributed to the moderate doping of their epitaxial Si of $\sim 1 \times 10^{15}$ cm^{-3}. Similarly, it is expected that the PCE of our hybrid SiNWs cell using a 15 μm Si absorber will improve if a moderate doping concentration is used.

4. CONCLUSION

In conclusion, we have demonstrated a simple and wafer-scalable process to fabricate high-efficiency SiNWs hybrid solar cells based on electroless etched SiNWs and transparent small molecule Spiro-OMeTAD. The effects of the SiNWs length on the cell performance have been investigated. It is found that cells with shorter SiNWs of 0.35 μm achieved the highest PCE of 9.92% under simulated AM 1.5G solar irradiation. The efficiency will be raised to 11.3% if the silver grids covered area is not considered. Even though the cells with longer SiNWs exhibit lower reflectance, their PCE are limited by higher carriers recombination owing to the increased SiNWs aggregation. We also found that the SiNWs hybrid cells with higher substrate doping concentration have their IPCE suppressed near the infrared spectrum because of bulk recombination. However, a PCE of 3.2% and a promising current density of 19 mA/cm^2 were achieved for cells fabricated on a heavier doped Si substrate with a diffusion length of only 15 μm. The PCE is expected to be improved when a Si thin film with moderate doping is applied. The fabrication process demonstrated here could be potentially adapted to Si thin film deposited on low-cost or flexible substrates, and thus suggests a potential approach to realizing portable, low-cost and efficient SiNWs/organic hybrid cells.

AUTHOR INFORMATION

Corresponding Author

*E-mail: erusli@ntu.edu.sg.

Notes

The authors declare no competing financial interest.

ACKNOWLEDGMENTS

This work was supported by A*STAR Singapore under grant No: 092 101 0055.

REFERENCES

(1) Bozhi, T.; Xiaolin, Z.; Kempa, T. J.; Ying, F.; Nanfang, Y.; Guihua, Y.; Jinlin, H.; Lieber, C. M. *Nature* **2007**, *449*, 885−889.
(2) Peng, K.-Q.; Xu, Y.; Wu, Y.; Yan, Y.; Lee, S.-T.; Zhu, J. *Small* **2005**, *1*, 1062−1067.
(3) Peng, K.-Q.; Wang, X.; Wu, X.-L.; Lee, S.-T. *Nano Lett.* **2009**, *9*, 3704−3709.
(4) Garnett, E. C.; Yang, P. *J. Am. Chem. Soc.* **2008**, *130*, 9224−9225.
(5) Garnett, E.; Yang, P. *Nano Lett.* **2010**, *10*, 1082−1087.
(6) Sivakov, V.; Andra, G.; Gawlik, A.; Berger, A.; Plentz, J.; Falk, F.; Christiansen, S. H. *Nano Lett.* **2009**, *9*, 1549−1554.
(7) Shiu, S.-C.; Chao, J.-J.; Hung, S.-C.; Yeh, C.-L.; Lin, C.-F. *Chem. Mater.* **2010**, *22*, 3108−3113.
(8) Zhang, F.; Sun, B.; Song, T.; Zhu, X.; Lee, S. *Chem. Mater.* **2011**, *23*, 2084−2090.
(9) He, L.; Jiang, C.; Rusli; Lai, D.; Wang, H. *Appl. Phys. Lett.* **2011**, *99*, 021104−6.
(10) Kayes, B. M.; Atwater, H. A.; Lewis, N. S. *J. Appl. Phys.* **2005**, *97*, 114302−1.
(11) Kelzenberg, M. D.; Boettcher, S. W.; Petykiewicz, J. A.; Turner-Evans, D. B.; Putnam, M. C.; Warren, E. L.; Spurgeon, J. M.; Briggs, R. M.; Lewis, N. S.; Atwater, H. A. *Nat. Mater.* **2010**, *9*, 239−244.
(12) Lu, H.; Gang, C. *Nano Lett.* **2007**, *7*, 3249−3252.
(13) Junshuai, L.; HongYu, Y.; She Mein, W.; Gang, Z.; Xiaowei, S.; Lo, P. G. Q.; Dim-Lee, K. *Appl. Phys. Lett.* **2009**, *95*, 033102.
(14) Huynh, W. U.; Dittmer, J. J.; Alivisatos, A. P. *Science* **2002**, *295*, 2425−2427.
(15) Jung-Chul, L.; Wonjoo, L.; Sung-Hwan, H.; Tae Geun, K.; Yun-Mo, S. *Electrochem. Commun.* **2009**, *11*, 231−234.
(16) Unalan, H. E.; Hiralal, P.; Kuo, D.; Parekh, B.; Amaratunga, G.; Chhowalla, M. *J. Mater. Chem.* **2008**, *18*, 5909−5012.
(17) Kalita, G.; Adhikari, S.; Aryal, H. R.; Afre, R.; Soga, T.; Sharon, M.; Koichi, W.; Umeno, M. *J. Phys. D. Appl. Phys* **2009**, *42*, 115104−8.
(18) He, L.; Rusli; Jiang, C.; Wang, H.; Lai, D. *IEEE Electr. Device Lett.* **2011**, *32*, 1406−1408.
(19) Syu, H.-J.; Shiu, S.-C.; Lin, C.-F. *Sol. Energy Mater. Sol. Cells* **2012**, *98*, 267−272.
(20) Lu, W.; Chen, Q.; Wang, B.; Chen, L. *Appl. Phys. Lett.* **2012**, *100*, 023112−5.
(21) Mayer, A. C.; Scully, S. R.; Hardin, B. E.; Rowell, M. W.; McGehee, M. D. *Mater. Today* **2007**, *10*, 28−33.
(22) Shaw, P. E.; Ruseckas, A.; Samuel, I. D. W. *Adv. Mater.* **2008**, *20*, 3516−3520.
(23) Scully, S. R.; McGehee, M. D. *Appl. Phys. Lett.* **2006**, *100*, 34907−1.
(24) Snaith, H. J.; Humphry-Baker, R.; Chen, P.; Cesar, I.; Zakeeruddin, S. M.; Gratzel, M. *Nanotechnology* **2008**, *19*, 424003−424014.
(25) Ding, I. K.; Tetreault, N.; Brillet, J.; Hardin, B. E.; Smith, E. H.; Rosenthal, S. J.; Sauvage, F.; Gratzel, M.; McGehee, M. D. *Adv. Funct. Mater.* **2009**, *19*, 2431−2436.
(26) Kroeze, J. E.; Hirata, N.; Schmidt-Mende, L.; Orizu, C.; Ogier, S. D.; Carr, K.; Gratzel, M.; Durrant, J. R. *Adv. Funct. Mater.* **2006**, *16*, 1832−1838.
(27) Spurgeon, J. M.; Atwater, H. A.; Lewis, N. S. *J. Phys. Chem. C* **2008**, *112*, 6186−6193.
(28) Shen, X.; Sun, B.; Yan, F.; Zhao, J.; Zhang, F.; Wang, S.; Zhu, X.; Lee, S. *ACS Nano* **2010**, *4*, 5869−5876.
(29) Peng, K.-Q.; Lee, S.-T. *Adv. Mater.* **2011**, *23*, 198−215.
(30) Shiu, S.-C.; Lin, S.-B.; Hung, S.-C.; Lin, C.-F. *Appl. Surf. Sci.* **2011**, *257*, 1829−1834.
(31) Tyagi, M. S.; Van Overstraeten, R. *Solid State Electron.* **1983**, *26*, 577−597.